Journal of
Mechanics of
Materials and Structures

NONLINEAR VIBRATION OF AN EDGE-CRACKED BEAM WITH A COHESIVE ZONE, I: NONLINEAR BENDING LOAD-DISPLACEMENT RELATIONS FOR A LINEAR SOFTENING COHESIVE LAW

Prasad S. Mokashi and Daniel A. Mendelsohn

Volume 3, Nº 8 October 2008

mathematical sciences publishers

JOURNAL OF MECHANICS OF MATERIALS AND STRUCTURES
Vol. 3, No. 8, 2008

NONLINEAR VIBRATION OF AN EDGE-CRACKED BEAM WITH A COHESIVE ZONE, I: NONLINEAR BENDING LOAD-DISPLACEMENT RELATIONS FOR A LINEAR SOFTENING COHESIVE LAW

PRASAD S. MOKASHI AND DANIEL A. MENDELSOHN

Part I of this paper describes the computations of the quasistatic nonlinear moment-slope relation for an edge-cracked beam element with a strictly linear softening cohesive zone ahead of the crack tip. A static plane stress linear elastic boundary element analysis is used in which the cohesive nonlinearity appears in the crack plane boundary conditions only. An iterative solution scheme is used to determine the unknown cohesive zone length, the cohesive displacement jumps, and the bending mode J-integral. Interpreting the moment-slope relation as a generalized load-displacement relation the bending compliance (and slope) at a given applied moment are calculated from computed J-integral values over a grid of applied moment and crack-length values. The dependence of the moment-slope relation on the cohesive law parameters is studied and the various computed moment-slope relations are then used in Part II to model the dynamic effect of the cohesive zone and law on the free-vibration of an edge-cracked simply-supported beam.

1. Introduction

The major kinematic effect of an edge-crack in a beam is the discontinuity the crack allows in both the net rotation and the net transverse deflection across the crack plane, Figure 1. The discontinuities are resisted by the bonded ligament in an elastic manner if the crack is in small-scale yielding. This allows the use of linear massless rotational and/or shear springs to represent the crack plane in thin structures with through cracks. The idea originated with the line-spring model of Rice and Levy [1972] applied to a static analysis of a through crack in a plate in bending. The model relates the jumps in the rotation $\Delta\theta$ and the jump in transverse deflection Δv to the applied bending moment M and the shear force Q at the crack plane, respectively. For cracks in small-scale yielding for which linear elastic fracture mechanics (LEFM) applies, the spring stiffnesses (or their reciprocals, the compliances) may be found from a two-dimensional elastic analysis of a cracked beam shaped geometry as found in many fracture mechanics handbooks [Tada et al. 1973; Yokoyama and Chen 1998] as a function of crack length, beam depth, and elastic properties. If the crack tip is attended by a cohesive zone, then the extent of the zone and the plastic stretch in the cohesive zone depend on the load which causes the stiffness (compliance) to depend on the load and the load-displacement relation to be nonlinear. The purpose of this paper is to compute the nonlinear bending load-displacement relation (moment-slope relation) for an edge-crack with a linear softening cohesive law and to study how it depends on the cohesive law parameters.

Keywords: cohesive zone, linear softening, compliance, J-integral, nonlinear load-displacement.

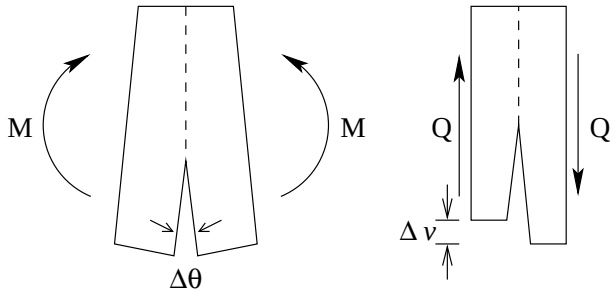

Figure 1. Left: Jump in slope $\Delta\theta$ at the crack plane due to the bending moment M. Right: Jump in deflection Δv at the crack plane due to the shear force Q.

Fracture process zones are typically characterized by nonlinear softening behavior in which the crack plane stress decreases with increasing irreversible deformation of the process zone. The particular relationship between the cohesive traction and the deformation is known as the cohesive or softening law. The softening zone is in general surrounded by a nonlinear plastic hardening region. Four general situations may be delineated. (i) Both the softening and hardening regions are small compared to the K-dominant region surrounding the crack tip, in which case LEFM is appropriate. (ii) The softening zone is small and is surrounded by a large plastic hardening zone, in which case elastic-plastic fracture mechanics is appropriate. (iii) Both the softening zone near the crack plane and the plastic hardening zone are appreciably large, in which case both cohesive zones and a plastic hardening region need to be modeled. (iv) The softening zone is confined to a region near the crack plane and is large compared to a negligible small region of plastic hardening which surrounds the softening zone. This requires a model with only an infinitesimally thin cohesive zone surrounded by elastic material. Typically (i) is referred to as brittle behavior, (ii) and (iii) are ductile behavior, and (iv) is quasibrittle behavior. The present work is concerned with the latter category, which is exhibited by a variety of materials: concrete, rock, ice, certain sands and clays, toughened ceramics, fibrous composites, brittle matrix composites, and a variety of bonded joint geometries and types (adhesive, weld, solder) [Hillerborg et al. 1976; Petersson 1981; González et al. 2004; Cox et al. 1989; Sensmeier and Wright 1989; Bao and Suo 1992; Suo et al. 1993; Botsis and Beldica 1994; Zok and Hom 1990; Bosco and Carpinteri 1995; Bao and McMeeking 1995; Xu et al. 1995; Fett et al. 1995; 1994; Anderson and Stigh 2004; Shetty and Spearing 1997; Yang et al. 1999; Cavalli et al. 2005; Yang et al. 2004; Sorensen 2002; Plaut and Ritchie 2004; Wei and Hutchinson 1998].

Cohesive zones were first introduced into the mathematical analysis of the crack problem nearly simultaneously by Dugdale [1960], Bilby et al. [1963], and Barenblatt [1962], for application to ductile metals. These original analyses assumed that the cohesive stress is constant over the entire cohesive zone. Hillerborg et al. [1976] applied cohesive modeling to quasibrittle materials like concrete and were the first to introduce a softening cohesive law in which after reaching a peak, the cohesive traction reduces as the plastic stretch increases. Many of the studies referenced in the previous paragraph note that all or a significant part of the cohesive law is in a softening mode. Linear and bilinear softening cohesive models have also been used, for example, by Geubelle and Rice [1995], Yang and Ravi-Chandar [1996], and Bažant and Planas [1998] for metals, concrete, and other quasibrittle materials. Exponential and other

nonlinear softening models have been used by Geubelle and Baylor [1998], Bažant and Li [1997], Li and Bažant [1997], Panasyuk and Yarema [2001], and Panasyuk et al. [2003] in the context of quasibrittle materials. Linear softening models have been used in boundary element formulations by Ohtsu and Chahrour [1995] and Aliabadi [1997] for quasibrittle materials like concrete to study crack propagation. Hanson and Ingraffea [2003] and Hanson et al. [2004] have used linear and bilinear softening cohesive models in numerical crack growth simulations in concrete using the finite element method.

From the work cited above it is clear that cohesive zones occur in many real material systems and that the use of cohesive zone models in computational settings is convenient, useful and prevalent today. Virtually all methods in the literature for determining the form or parameters of a cohesive law for a particular material have been based on destructive testing to failure. This includes all of the work cited above in which this crucial parameter identification is actually carried out. The present work is one of two parts in an effort to develop a nondestructive technique for characterizing the cohesive law of a structural material, or in the case of an interface crack, the cohesive law of the bond or interface material itself. The characterization is based on the nonlinear vibration response of a model of an edge-cracked beam in which the crack plane is replaced by a bending spring and a transverse shear spring and the beam is modeled using Euler–Bernoulli beam theory. Assuming nonlinear behavior in bending only, the spring stiffnesses are calculated in this part of the paper from two-dimensional fracture mechanics solutions for beam like geometries with edge-cracks and mode I cohesive zones. The second part of the paper uses these stiffnesses in a nonlinear beam vibration analysis. In this way the forward problem is posed and solved: that is, for a given cracked beam and cohesive law, the nonlinear beam vibration response at a prescribed static preload is predicted. The eventual goal is to solve the inverse problem of interpreting measured nonlinear vibratory response to ascertain the parameters of a cohesive law for a known crack length and superimposed static preload. The rationale for the assumption of a static preload is given in detail in the second part of the paper.

Specifically the objective of the first part of the paper is to develop a methodology for computing the nonlinear generalized load-displacement (moment-slope) relationship in a two dimensional edge-cracked beam-like geometry with a linear softening cohesive crack ahead of the crack tip subjected to pure bending. The nonlinear spring stiffness for use in the beam vibration analysis is calculated from the nonlinear moment-slope relationship. The analysis begins by solving the crack and cohesive zone boundary value problem using a two-body, iterative, direct boundary element method (BEM). By virtue of the method of solution the results also apply to the situation of two beams bonded together with an edge crack in the plane of the bond. For each softening law studied, the J-integral is obtained from the BEM analysis for a range of crack lengths and applied moments. Then, using the relationship between the J-integral and generalized load and displacement (bending moment and jump in slope across the crack plane) for the cracked geometry, the compliance is derived in terms of the J-integral. Once the compliance is found at a given load the generalized displacement (jump in slope across the crack) may be calculated. This yields the predicted generalized load versus the displacement relationship, which is in turn used in the nonlinear beam vibration analysis presented in the second part of this paper.

The paper starts with a discussion of crack plane compliance and the J-integral and their relationship. This is followed by the BEM formulation and some results on the dependence of the cohesive response on the loading and the cohesive law parameters. Next we describe the numerical analysis for obtaining the generalized load versus displacement relation, and present the curves for a variety of cohesive laws.

2. Crack plane compliance and the J-integral

For an Euler–Bernoulli beam of rectangular cross section and containing a through-surface edge-crack, if axial forces are neglected and only shear and bending loads are considered, then the crack plane is subjected to a net shear force Q and a net bending moment M. The presence of a crack causes a relative jump in displacement and rotation of one flank of the crack relative to the other as shown in Figure 1 for a cracked element in an edge-cracked beam. $\Delta\theta$ represents the jump in slope and Δv represents the jump in the displacement. The increased compliance due to the presence of the crack can be lumped into a continuous spring of zero width that connects the two faces of the crack [Rice and Levy 1972]. If the beam is now divided at the crack plane into two regions and the crack plane replaced by line(planar)-springs of zero-width, the compliance relations for the line-springs may be written as

$$\Delta\theta = \theta_2 - \theta_1 = \lambda_\theta M, \tag{1}$$

$$\Delta v = v_2 - v_1 = \lambda_v Q, \tag{2}$$

where λ_θ and λ_v are the compliances due to bending moment and shear force respectively. The springs relate the shear force and bending moment to the jump in deflection and rotation, respectively, across the crack plane. Treating each of these as global or generalized load and load-point displacement pairs, basic fracture mechanics principles state that the bending compliance can be written in terms of J_{I}, the mode I contribution to the J-integral, as [Kanninen and Popelar 1985]

$$\lambda_\theta(\bar{M}, \bar{a}) = \frac{W}{b}\frac{1}{\bar{M}}\int_0^{\bar{a}} \frac{\partial J_{\mathrm{I}}(\bar{M}, \bar{a})}{\partial \bar{M}}\, d(\bar{a}). \tag{3}$$

and similarly that the shear compliance may be written in terms of J_{II}, the mode II contribution to the J-integral as

$$\lambda_v(\bar{Q}, \bar{a}) = \frac{W}{b}\frac{1}{\bar{Q}}\int_0^{\bar{a}} \frac{\partial J_{\mathrm{II}}(\bar{Q}, \bar{a})}{\partial \bar{Q}}\, d(\bar{a}). \tag{4}$$

Since in the present two-dimensional setting J_{I} is actually a function of applied moment per unit thickness and nondimensional crack length to beam depth ratio, we have introduced normalized applied loads and crack length $\bar{M} \equiv M/b$, $\bar{Q} \equiv Q/b$, and $\bar{a} \equiv a/W$. Here b is the (out of plane) beam thickness, a is the crack length, and W is the beam depth; see Figure 2. If the crack tip is elastic or in small-scale yielding (negligible cohesive zone size) then the compliance relations are linear, the compliances are independent of applied loads, and the J-integral components are proportional to their respective applied load. The J-integral components and the compliances may in this case be written directly in terms of the stress-intensity factors, which are well-tabulated for edge-cracked specimens [Yokoyama and Chen 1998; Tada et al. 1973; Wilson 1970; Tharp 1987]. However, if there is cohesive damage ahead of the crack tip then the J-integral components depend nonlinearly on the applied load and the integrals in (3) or (4) must be used. This requires that the J-integral be evaluated at a fairly fine grid of applied load and crack-length values [Mendelsohn 2006]. For convenience, the present analysis confines the nonlinearity to the bending spring, and hence the shear compliance can be calculated from the formulas in [Yokoyama and Chen 1998]. The focus from here on in this paper is then on the nonlinear bending compliance in (3) and the resulting nonlinear $\bar{M}$–$\Delta\theta$ relation. This requires only the consideration of bending loading leading to mode I loading at the crack tip. The J-integral, which appears in (3), is computed from results

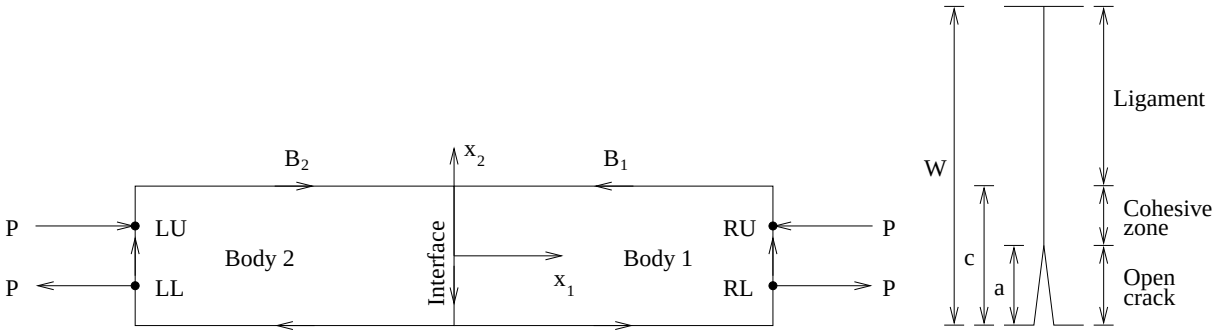

Figure 2. Left: Boundary element geometry showing the crack plane as the interface between two fictitious bodies having boundaries B_1 and B_2. The couples at the ends load the model in bending (mode I). Right: Interface divided into three regions.

from a two-dimensional elastostatic BEM analysis of an edge-crack with a planar cohesive zone in a beam shaped homogeneous elastic solid subjected to edge-moments as shown in Figure 2, left. The elastic crack tip is a distance a from the bottom of the beam and the end of the cohesive zone is a distance c from the bottom of the beam, Figure 2, right. The cohesive law is the relationship between the normal traction t and the cohesive stretch δ in the cohesive zone which is modeled by a jump in normal displacement across the crack plane:

$$\delta = u_1^{x_1=0^+} - u_1^{x_1=0^-}, \tag{5}$$

where u_1 denotes displacement in the x_1 direction normal to the crack plane. δ_t is the value of δ at $x_2 = -\frac{1}{2}W + a$; see Figure 3, left. A linear softening cohesive law is shown in Figure 3, right, and is written as

$$t(\delta) = t_0\left[1 - \frac{\delta}{\delta_0}\right], \tag{6}$$

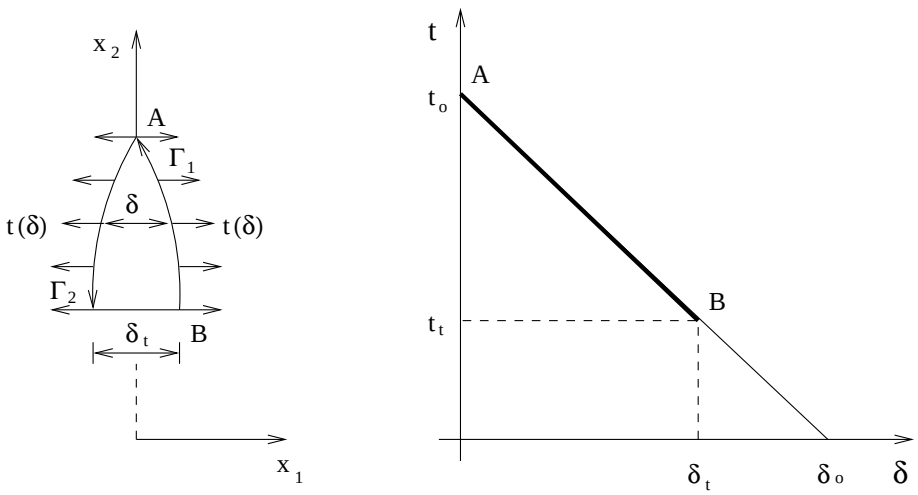

Figure 3. Left: Free body diagram of the cohesive zone. Right: Linear softening cohesive law showing the extent of softening.

where t_0 is the peak cohesive traction and δ_0 is the critical value of cohesive crack opening displacement at which extension of the elastic crack tip or crack growth occurs. The focus is on obtaining the cohesive response to loadings such that the entire cohesive law is exercised, but crack growth does not occur. Following the development in [Kanninen and Popelar 1985] but replacing the Dugdale cohesive law, for which the traction is constant and equal to t_0 over the entire cohesive zone, with the linear softening law in (6) we obtain

$$J_{\mathrm{I}} = \int_0^{\delta_t} t(\delta)\, d\delta = t_0 \delta_t \left[1 - \frac{1}{2} \frac{\delta_t}{\delta_0} \right], \tag{7}$$

which is the area under the exercised portion of the cohesive law. We restrict δ_t to be less than its value at crack growth δ_0. As δ_t approaches δ_0, J_{I} approaches the critical value for crack growth, $J_{\mathrm{I}0} = \frac{1}{2} t_0 \delta_0$, a third parameter in addition to t_0 and δ_0 which can be used to characterize the cohesive law. Crack growth is not modeled in order to keep the envisioned free-vibration experiments as simple as possible. The crack tip opening displacement δ_t is solved for using a two-body, iterative, direct boundary element formulation for an edge crack in a beam shaped solid subjected to pure bending, and the corresponding J-integral from (7).

3. Boundary element formulation and solution scheme

The beam shaped geometry with an edge crack subjected to pure bending is shown in Figure 2, left. The total length L of the beam is taken large enough compared to W to make the crack tip fields independent of any end effects at the load points and for this two-dimensional elasticity model to behave like an Euler–Bernoulli beam. The beam is further divided into two fictitious bodies with the crack plane as the interface between them. The interface is divided into three regions: (i) ligament, (ii) cohesive zone - with a linear softening $t - \delta$ law, and (iii) open crack as shown in Figure 2, right. B_1 and B_2 represent the boundaries of the two bodies that are discretized into elements with constant tractions and displacements. The direct boundary element formulation is applied to each of the two bodies which make up the beam under consideration. Discretizing B_1 and B_2 into N elements each, for each body ($k = 1, 2$) the reciprocal identity gives the two matrix equations

$$[{}_k U_{ij}][{}_k t_j] + [{}_k T_{ij}][{}_k u_j] = [0], \qquad k = 1, 2. \tag{8}$$

The boundary traction and displacement N-vectors are $[{}_k t_j]$ and $[{}_k u_j]$, where the leading subscript refers to the body and the trailing subscript refers to the direction of traction or displacement. $[{}_k T_{ij}]$ and $[{}_k U_{ij}]$ with $i, j = 1, 2$ are the infinite space Green's matrices for tractions and displacements, respectively in body k. Details of these matrices can be found in [Brebbia and Dominguez 1989] and in the present notation in the doctoral thesis by Young [1994]. The boundary conditions in the crack plane are now described. The bending loading considered leads to a mode I cohesive zone only. A complete formulation with mode I and II cohesive behavior has also been completed and used in the cracked bimaterial beam problem [Mokashi 2007], but is not presented here. Starting with the ligament, normal, and tangential displacements across the fictitious interface are continuous and normal and shear tractions are equal and opposite (stresses are continuous). In the cohesive zone the tangential displacement and the shear traction are continuous across the interface, just as they are in the ligament, while the normal tractions are equal and opposite on either side of the interface and related to the normal displacement jump through the

cohesive law, (6). In the open crack both the normal and shear tractions on either crack surface are zero. The open crack surfaces and the boundaries B_1 and B_2 (except the load points) are traction free. The point loads creating the couples are modeled as constant applied normal traction over the element at whose node they act. These boundary conditions give rise to a $4N \times 4N$ linear system in the remaining unknown tractions and displacements. The matrix equation corresponding to each boundary condition consists of all rows of each of the Green's submatrices and only those columns corresponding to the node at which the boundary condition is applied. The details of the matrices that give rise to the final linear system can be found in the doctoral thesis by Mokashi [2007]. In addition to the $4N$ unknown tractions and displacements, the length of the cohesive zone is also unknown.

An automatic iterative solution scheme is employed to obtain the unknown tractions and displacements and the extent of the cohesive zone. The scheme begins with an initial guess of the number of elements that constitute the extent of the cohesive zone. The evaluated normal traction value in an element of the cohesive zone nearest to the ligament is then compared with t_0. If it is larger than t_0, iterations are performed on the number of elements in the cohesive zone until the value of the normal traction in the first element of the ligament, nearest to the cohesive zone, is less than t_0. The other constraint for the solution is that in the open crack there is no interpenetration of material, that is, the crack exhibits opening displacements only. The solution for displacements is automatically checked for this condition. A representative solution for the normal tractions and displacements at the interface under predominantly mode-I conditions is shown in Figure 4. The interface is composed of 100 elements which provides a sufficient amount of refinement to obtain convergent results. The markers in the rightmost pane of the figure show the traction values in the elements in the cohesive zone, thus indicating the extent to which

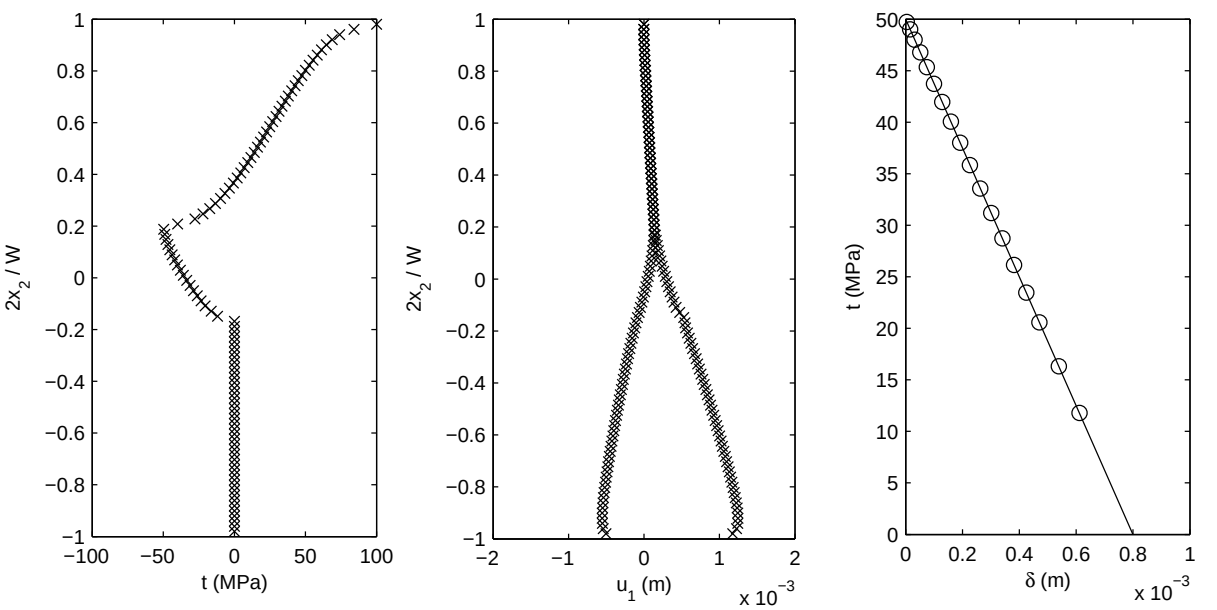

Figure 4. Representative solution for tractions and displacements in the cohesive zone along with the extent of softening ($E = 72800$ MPa, $\nu = 0.3$, $W = 12.5$ mm, $a/W = 0.42$, $\bar{M} = 800.78$ N, $t_0 = 50$ MPa, and $\delta_0 = 0.0008$ m).

the linear cohesive softening law has been exercised (how close δ_t is to δ_0) and the number of elements in the cohesive zone, and hence its length. The element nearest the crack tip has the smallest traction and largest displacement δ_t, while the traction approaches t_0 and the displacement goes to zero at the end of the cohesive zone. In this example the elastic crack is 42 elements long, the cohesive zone is 18 elements long, and δ_t is about 75% of its critical value. The solution shown in Figure 4 is for a material with shear modulus $G = 28,000$ MPa, Poisson's ratio $\nu = 0.3$ and the cohesive law is $t_0 = 50$ MPa and $\delta_0 = 0.0008$ m. In all simulations W is chosen to be 12.5 mm. The total number of elements on the boundaries of both the bodies is 840 making the total size of the linear system 1680×1680.

4. Extent of cohesive zone and softening

Several linear softening cohesive laws with three basic kinds of parameter variations are considered in this section. For each, the beam is quasistatically loaded such that significantly large cohesive zones are formed ahead of the crack tip. For a given peak cohesive traction and displacement the nonlinear $\bar{M}$–$\Delta\theta$ relation is obtained over a range of applied moment per unit thickness that exercises the linear softening cohesive law as much as possible, which in turn creates as large as possible cohesive zones, both without crack growth. Before obtaining the load-displacement relations we discuss the dependence of each of these features of the cohesive behavior on the applied moment, peak cohesive traction t_0, critical opening displacement δ_0, and the critical J-integral, J_{I0}.

First, as expected, for a given cohesive law and at a given crack length, as the applied moment is increased the cohesive zone length increases as well. When several linear softening cohesive laws having the same value of t_0 and different values of δ_0 are considered, it is observed that for a given crack length and applied moment smaller cohesive zones are formed for the steeper cohesive laws compared to the less steep cohesive laws. As δ_t for the steepest cohesive law approaches its critical value, cohesive zones just begin to form for the less steep cohesive laws. The length of the cohesive zone as it approaches δ_0 is very small for the steepest cohesive law. Now if several cohesive laws with different values of t_0 and the same value of δ_0 are considered then for a given crack length and applied moment the size of the cohesive zone is significantly smaller for the more steep cohesive law compared to the less steep cohesive law. Longer cohesive zones are obtained as δ_t approaches δ_0 for the least steep cohesive law. Similar trends are obtained when several cohesive laws having the same value of J_{I0}, but different values of t_0 and δ_0, are considered. As the softening curve becomes steeper the size of the cohesive zone becomes markedly smaller, whereas for the less steep cohesive laws very long cohesive zones are obtained. Details of the trends are found in [Mokashi 2007].

A representative variation of the dimensionless J-integral, J/J_{I0} with dimensionless crack length a/W for various values of the applied moment per unit thickness $\bar{M}$ is shown in Figure 5. The cohesive law on which these results are based is $t_0 = 50$ MPa, $\delta_0 = 1.8(10^{-}3)$ m, and $J_{I0} = 45(10^3)$ N/m. Similar results for several cohesive laws are also found in [Mokashi 2007].

5. Numerical analysis for obtaining nonlinear load-displacement curves

The nonlinear $\bar{M}$–$\Delta\theta$ curves for a given crack length are found by first obtaining the bending compliance λ_θ as a function of applied moment by evaluating the integral in (3). Noting that the integral is over crack length, this requires knowledge of $dJ/d\bar{M}$ over a grid of applied moment and crack length values. Next

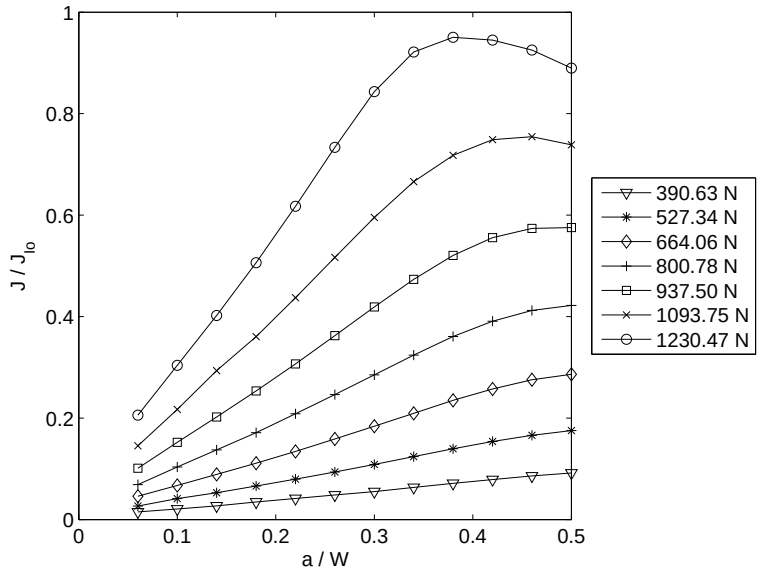

Figure 5. Variation of the dimensionless J-integral (J/J_{I0}) with the dimensionless crack length (a/W) at various values of the normalized moment $\bar{M}$ (as indicated by the markers in the legend). $t_0 = 50\,\mathrm{MPa}$, $\delta_0 = 0.0018\,\mathrm{m}$ and $J_{\mathrm{I0}} = 45(10^3)\,\mathrm{N/m}$.

$\Delta\theta$ is found from (1) for a range of values of $\bar{M}$ and the calculated λ_θ. At a given crack length a/W the analysis starts by using Newton's method to obtain the interpolation polynomial $J_{N-1}(\bar{M})$ from the J-integral values obtained from the boundary element calculations at various values of applied moment $\bar{M}$:

$$J_{N-1}(\bar{M}) = \sum_{i=1}^{N} J\big[\bar{M}_1, \ldots, \bar{M}_i\big] \prod_{j=1}^{i-1} \big(\bar{M} - \bar{M}_j\big). \tag{9}$$

For N points in the original data, $J_{N-1}(\bar{M})$ is a polynomial of order $(N-1)$. The coefficients of this interpolating polynomial are obtained using divided differences in the standard way and are denoted by $J\big[\bar{M}_1, \ldots, \bar{M}_i\big]$ [Atkinson and Han 2004]. Using the original values of applied moment as the skeleton, a denser grid of moment values is created with many points between each of the original values. Using the interpolation polynomial, the values J_n are generated on this finer grid, where the index n ranges over this fine grid of values. The derivative in (3), $dJ/d\bar{M}$, is obtained using central differences. This procedure is repeated to obtain curves of $dJ/d\bar{M}$ at several crack lengths $\bar{a}$ that range between 0.06 and 0.5. At a given moment $\bar{M}$, an interpolating polynomial of order $(N-1)$ for $dJ/d\bar{M}$ as a function of $\bar{a}$, with values of J-integral at N crack lengths $\bar{a}$, can be written

$$\left(\frac{dJ(\bar{a})}{d\bar{M}}\right)_{N-1} = \sum_{i=1}^{N} \frac{dJ}{d\bar{M}}\big[\bar{a}_1, \ldots, \bar{a}_i\big] \prod_{j=1}^{i-1} \big[\bar{a} - \bar{a}_j\big]. \tag{10}$$

The coefficients of this interpolating polynomial are again obtained using divided differences and are denoted by $\frac{dJ}{d\bar{M}}\big[\bar{a}_1, \ldots, \bar{a}_i\big]$. Using the polynomial functions for $\frac{dJ}{d\bar{M}}(\bar{a})$ obtained at several values of $\bar{M}$, several data points $(dJ/d\bar{M})_n$ are now created at multiple values of crack lengths $\bar{a}_n$ for crack lengths

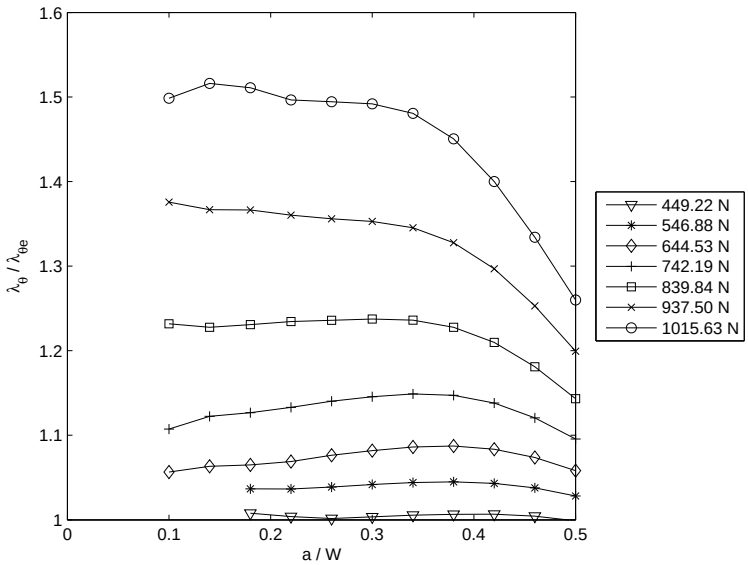

Figure 6. Dimensionless compliance ($\lambda_\theta/\lambda_{\theta e}$) curves with dimensionless crack length a/W. $t_0 = 50$ MPa and $J_{I0} = 45(10^3)$ N/m. The values in the legend represent various normalized moments $\bar{M}$.

ranging from 0 to 0.5. The integral in (3) over crack length is, at a given moment $\bar{M}$, obtained numerically using the trapezoidal rule. The final expression then for λ_θ can be written as

$$\lambda_\theta = \frac{W}{b}\frac{1}{\bar{M}}\sum_{i=1}^{n}\frac{1}{2}\left[\left(\frac{dJ(\bar{a})}{d\bar{M}}\right)_i + \left(\frac{dJ(\bar{a})}{d\bar{M}}\right)_{i+1}\right]h_{\bar{a}}. \tag{11}$$

where $h_{\bar{a}}$ denotes the increment in crack length $\bar{a}$. The variation of the dimensionless compliance $\lambda_\theta/\lambda_{\theta e}$ with dimensionless crack length $\bar{a}$ is shown in Figure 6.

The curves are for various values of moment ratio M_R obtained using a set of values of the J-integral corresponding to the cohesive law ($t_0 = 50$ MPa, $J_{I0} = 45(10^3)$ N/m) used to generate the curves in Figure 5. The normalization constant $\lambda_{\theta e}$ is the elastic compliance obtained using a set of values of the J-integral for the same beam geometry without considering a cohesive zone ahead of the crack tip. The J-integral for the linear elastic case is obtained in the standard way from the stress intensity factor K_I that is evaluated from the near tip stress fields using a similar boundary element code [Young 1994]. The numerical scheme just discussed is used to obtain the elastic compliance $\lambda_{\theta e}$ from those boundary element results. For reference purposes, the variation of the elastic compliance with crack length is shown in Figure 7.

The normalization is used because both the cohesive and elastic compliances are proportional to (W/b). Figure 6 shows that at higher crack lengths the increase in compliance due to cohesive deformation ahead of the crack tip is less pronounced than at lower crack lengths. This is due to the almost pure bending like applied stress distribution on the crack plane. For a crack length of half the depth the entire cohesive zone lies in a region of what would be compressive normal stress in the absence of the crack. This effect is more dominant at higher values of applied moment $\bar{M}$ and affects the elastic compliance for the same

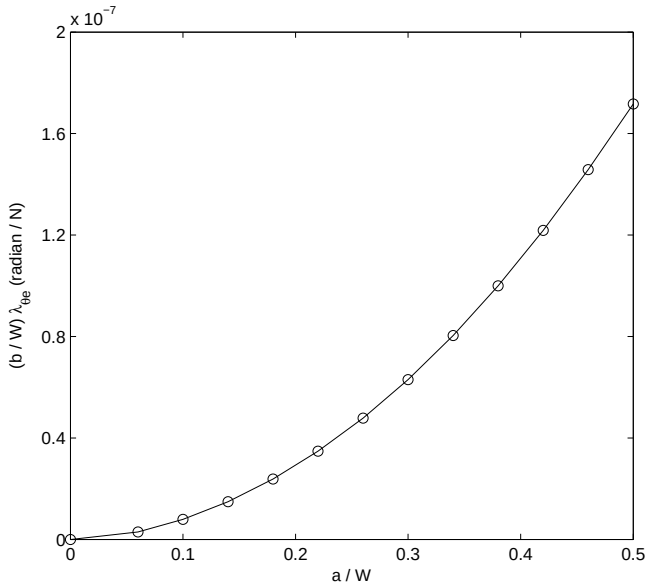

Figure 7. Variation of elastic compliance ($\lambda_{\theta e}$) with dimensionless crack length a/W.

geometry much less as long as the crack tip itself is below the mid-plane. At very low crack lengths and at low load levels the values of compliance are not reliable due to the inaccuracies in the cohesive zone size and in numerically obtaining the derivative $dJ/d\bar{M}$. Only reliable results are reported. Over a middle range of crack lengths the results show consistently that the elastic compliance accounts essentially for the crack length effect and that the additional increase in compliance due to cohesive stretching depends primarily on the applied moment and not on the crack length itself. The dependence of the normalized compliance on the applied moment at a given crack length is itself nonlinear. In order for the compliance to be about 10% larger than the elastic, the load must be 65% more than the elastic moment. But, as the load increases the rate of increase in the inelastic compliances increases and a 50% increase in the inelastic compliance occurs for a shorter crack at 125% more load than the elastic moment.

At a given crack length the jump in rotation $\Delta\theta$ is evaluated by solving (1) at the N discrete calculated values of the compliance, (11), at the chosen values of applied moment. To obtain a smooth $\bar{M}$–$\Delta\theta$ curve Newton's method of interpolation is used again to obtain a polynomial $\bar{M}_{N-1}(\Delta\theta)$ of order $(N-1)$

$$\left(\bar{M}(\Delta\theta)\right)_{N-1} = \sum_{i=1}^{N} \bar{M}[\Delta\theta_1, \ldots, \Delta\theta_i] \prod_{j=1}^{i-1} (\Delta\theta - \Delta\theta_j). \tag{12}$$

where $\bar{M}[\Delta\theta_1, \ldots, \Delta\theta_i]$ are the coefficients of the polynomial obtained by divided differences. Normalized $\bar{M}$–$\Delta\theta$ curves for the single specific cohesive law ($t_0 = 50$ MPa, $J_{I0} = 45(10^3)$ N/m) at several crack lengths are shown in Figure 8. $\Delta\theta_e$ represents the elastic value of $\Delta\theta$ at $\bar{a} = 0.5$ obtained from the elastic compliance.

To study the effect of the cohesive law parameters, t_0 and δ_0 on the $\bar{M}$–$\Delta\theta$ relationship, 11 cohesive laws in were considered; see Table 1 on the right. The present study is exploratory and intended to determine the feasibility of the overall nondestructive characterization scheme and is not tied to a particular

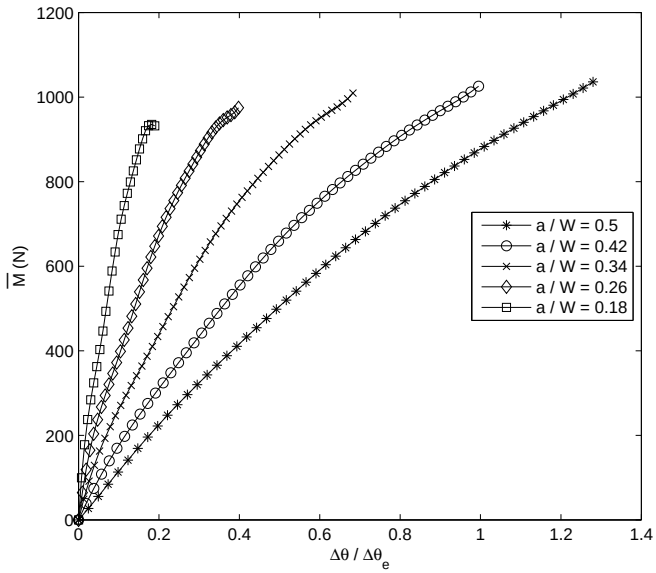

Figure 8. Normalized $\bar{M}$–$\Delta\theta$ curves at various crack lengths. $t_0 = 50$ MPa and $J_{I0} = 45(10^3)$ N/m.

material or cohesive process at this point. Therefore the parameter study was performed at only one value of Young's modulus and Poisson's ratio and a range of cohesive law parameters and applied moment such that the cohesive laws are well exercised, yet crack growth does not occur, that is, J does not exceed it's critical value J_{I0}. The critical J-integral values of all of the laws listed below are all less than, or of the order of magnitude of, the value corresponding to the critical stress intensity factor for LEFM crack growth of 60 MPa$\sqrt{m}$.

Figure 9 shows the $\bar{M}$–$\Delta\theta$ curves for the various cohesive laws in Table 1. All results are for a beam depth of 1.25 m by appropriate scaling. The curves are clearly grouped by the value of the peak cohesive traction t_0 and show an increase in $\Delta\theta$ for decreasing peak traction at a given moment. Within a group at a particular peak traction t_0 there is a slight dependence on the critical displacement δ_0 (or equivalently the critical J integral J_{I0}). The main feature of that dependence is that the values of the applied moment at which (a) the cohesive law just begins to be exercised, and (b) crack growth occurs both increase with increasing δ_0 (J_{I0}). These values of applied moment are the approximate limits of each of the $\bar{M}$–$\Delta\theta$ curves shown in Figure 9. These curves provide the properties of the springs used to represent the crack plane in the dynamic beam vibration analysis and are accurate enough to carry out a two-term Taylor series expansion of the data at a given static load level.

t_0	$\delta_0 = 0.8$ mm	$\delta_0 = 1.3$ mm	$\delta_0 = 1.6$ mm	$\delta_0 = 1.8$ mm
25 MPa		7 (16.3 N/m)	4 (20 N/m)	1 (22.5 N/m)
50 MPa	11 (20 N/m)	8 (32.5 N/m)	5 (40 N/m)	2 (45 N/m)
75 MPa		9 (48.8 N/m)	6 (60 N/m)	3 (62.5 N/m)

Table 1. Cohesive laws: the first number is the law number; the number in parentheses is J_{I0} for the law.

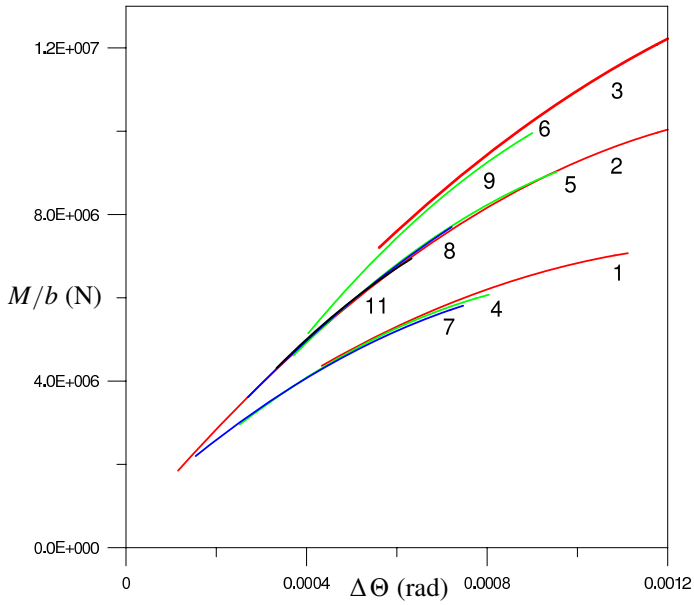

Figure 9. A plot of the $\bar{M}$–$\Delta\theta$ relationship for the cohesive laws in Table 1 for a dimensionless crack length of $a/W = 0.34$.

6. Conclusion

A BEM formulation for a linear softening cohesive zone problem in an edge cracked beam like geometry which requires an iterative process to determine the length of the cohesive zone to satisfy the nonlinear interfacial boundary conditions has been presented. The behavior of the cohesive zone with respect to the applied load, t_0, δ_0 and a/W has been examined for nonpropagating cracks. The iterative boundary element solution scheme is robust, as the extent of the cohesive zone along with the solution for tractions and displacements are generally obtained within 3–6 iterations with an arbitrary initial guess.

For a specific linear softening cohesive law applied to the edge cracked beam shaped geometry the variation of the J-integral calculated for various values of applied load and crack lengths a/W are used in an algorithm for generating the nonlinear $\bar{M}$–$\Delta\theta$ curves. These results have potential application in the characterization of the cohesive behavior ahead of a crack tip in vibration analysis as discussed in the second part of this paper. In particular, a nonlinear free-vibration analysis, using the nonlinear $\bar{M}$–$\Delta\theta$ curves in Figure 9, is developed for exploring the effect of cohesive law parameters on the magnitude of various nonlinear beam responses.

Finally we note that the results presented here apply equally to a crack in a homogeneous beam and to a crack in a weak interface or bond layer between two beam sections made of the same material. The BEM model for the problem of a cohesive crack in the interface or bond layer between two beam sections of dissimilar materials is the same as for the similar material case, except that even with strictly mode I loading, the material mismatch causes the cohesive behavior to be of a mixed mode nature and a new combined mixed-mode cohesive law has to be used. This is the subject matter of ongoing research.

References

[Aliabadi 1997] M. H. Aliabadi, "A new generation of boundary element methods in fracture mechanics", *Int. J. Fract.* **86**:1–2 (1997), 91–125.

[Anderson and Stigh 2004] T. Anderson and U. Stigh, "The stress-elongation relation for an adhesive layer loaded in peel using equilibrium of energetic forces", *Int. J. Solids Struct.* **41**:2 (2004), 413–434.

[Atkinson and Han 2004] K. Atkinson and W. Han, *Elementary numerical analysis*, 3rd ed., Wiley, Hoboken, NJ, 2004.

[Bao and McMeeking 1995] G. Bao and R. M. McMeeking, "Thermomechanical fatigue cracking in fiber reinforced metal-matrix composites", *J. Mech. Phys. Solids* **43**:9 (1995), 1433–1460.

[Bao and Suo 1992] G. Bao and Z. Suo, "Remarks on crack bridging concepts", *Appl. Mech. Rev.* **45**:8 (1992), 355–366.

[Barenblatt 1962] G. I. Barenblatt, "The mathematical theory of equilibrium cracks in brittle fracture", pp. 55–129 in *Advances in Applied Mechanics*, vol. 7, edited by H. L. Dryden and T. von Kármán, Academic Press, New York, 1962.

[Bažant and Li 1997] Z. P. Bažant and Y. Li, "Cohesive crack with rate-dependent opening and viscoelasticity, I: Mathematical model and scaling", *Int. J. Fract.* **86**:3 (1997), 247–265.

[Bažant and Planas 1998] Z. P. Bažant and J. Planas, *Fracture and size effect in concrete and other quasibrittle materials*, CRC Press, Boca Raton, FL, 1998.

[Bilby et al. 1963] B. A. Bilby, A. H. Cottrell, and K. H. Swinden, "The spread of plastic yield from a notch", *Proc. R. Soc. A* **272**:1350 (1963), 304–314.

[Bosco and Carpinteri 1995] C. Bosco and A. Carpinteri, "Discontinuous constitutive response of brittle matrix fibrous composites", *J. Mech. Phys. Solids* **43**:2 (1995), 261–274.

[Botsis and Beldica 1994] J. Botsis and C. Beldica, "Strength characteristics and fatigue crack growth in a composite with long aligned fibers", *Int. J. Fract.* **69**:1 (1994), 27–50.

[Brebbia and Dominguez 1989] C. A. Brebbia and J. Dominguez, *Boundary elements: an introductory course*, Computational Mechanics, Southampton, 1989.

[Cavalli et al. 2005] M. N. Cavalli, M. D. Thouless, and Q. D. Yang, "Cohesive-zone modelling of the deformation and fracture of spot-welded joints", *Fatigue Fract. Eng. Mater. Struct.* **28**:10 (2005), 861–874.

[Cox et al. 1989] B. N. Cox, M. R. James, D. B. Marshall, W. L. Morris, C. G. Rhodes, and M. Shaw, "Failure mechanisms in titanium aluminide/SiC composites", pp. 313 in *Proceedings of the* 10^{th} *International SAMPE Conference* (Birmingham), edited by S. Benson et al., Elsevier, Amsterdam, 1989.

[Dugdale 1960] D. S. Dugdale, "Yielding of steel sheets containing slits", *J. Mech. Phys. Solids* **8**:2 (1960), 100–104.

[Fett et al. 1994] T. Fett, D. Munz, C.-T. Yu, and A. S. Kobayashi, "Determination of bridging stresses in reinforced Al_2O_3", *J. Am. Ceram. Soc.* **77**:12 (1994), 3267–3269.

[Fett et al. 1995] T. Fett, D. Munz, G. Thun, and H.-A. Bahr, "Evaluation of bridging parameters in aluminas from R-curves by use of fracture mechanical weight function", *J. Am. Ceram. Soc.* **78**:4 (1995), 949–951.

[Geubelle and Baylor 1998] P. H. Geubelle and J. S. Baylor, "Impact-induced delamination of composites: a 2D simulation", *Compos. B Eng.* **29**:5 (1998), 589–602.

[Geubelle and Rice 1995] P. H. Geubelle and J. R. Rice, "A spectral method for three-dimensional elastodynamic fracture problems", *J. Mech. Phys. Solids* **43**:11 (1995), 1791–1824.

[González et al. 2004] C. González, J. LLorca, and A. Weck, "Toughness of fiber-reinforced titanium as a function of temperature: Experimental results and micromechanical modeling", *Acta Mater.* **52**:13 (2004), 3929–3939.

[Hanson and Ingraffea 2003] J. H. Hanson and A. R. Ingraffea, "Using numerical simulations to compare the fracture toughness values for concrete from the size-effect, two-parameter and fictitious crack models", *Eng. Fract. Mech.* **70**:7–8 (2003), 1015–1027.

[Hanson et al. 2004] J. H. Hanson, T. N. Bittencourt, and A. R. Ingraffea, "Three-dimensional influence coefficient method for cohesive crack simulations", *Eng. Fract. Mech.* **71**:15 (2004), 2109–2124.

[Hillerborg et al. 1976] A. Hillerborg, M. Modéer, and P.-E. Petersson, "Analysis of crack formation and crack growth in concrete by means of fracture mechanics and finite elements", *Cement Concrete Res.* **6**:6 (1976), 773–781.

[Kanninen and Popelar 1985] M. F. Kanninen and C. H. Popelar, *Advanced fracture mechanics*, Oxford University Press, New York, 1985.

[Li and Bažant 1997] Y. Li and Z. P. Bažant, "Cohesive crack model with rate-dependent opening and viscoelasticity, II: Numerical algorithm, behavior and size effect", *Int. J. Fract.* **86**:3 (1997), 267–288.

[Mendelsohn 2006] D. A. Mendelsohn, "Free vibration of an edge-cracked beam with a Dugdale–Barenblatt cohesive zone", *J. Sound Vib.* **292**:1–2 (2006), 59–81.

[Mokashi 2007] P. S. Mokashi, *Numerical modeling of homogeneous and bimaterial crack tip and interfacial cohesive zones with various traction-displacement laws*, Ph.D. thesis, The Ohio State University, 2007.

[Ohtsu and Chahrour 1995] M. Ohtsu and A. H. Chahrour, "Fracture analysis of concrete based on the discrete crack model by the boundary element method", pp. 335–347 in *Fracture of brittle disordered materials: Concrete, rock and ceramics*, edited by G. Baker and B. L. Karihaloo, E & FN Spon, London, 1995.

[Panasyuk and Yarema 2001] V. V. Panasyuk and S. Y. Yarema, "On the origin of the δ_k-model and the model of plastic strips", *Mater. Sci.* (*Russia*) **37**:2 (2001), 346–353.

[Panasyuk et al. 2003] V. V. Panasyuk, I. I. Luchko, and I. N. Pan'ko, "Deformation model of fracture in concrete", *Strength Mater.* **35**:2 (2003), 114–121.

[Petersson 1981] P. E. Petersson, "Crack growth and development of fracture zone in plain concrete and similar materials", Report TVBM-1006, Lund Institute of Technology, Lund, 1981.

[Plaut and Ritchie 2004] R. H. Plaut and J. L. Ritchie, "Analytical solutions for peeling using beam-on-foundation model and cohesive zone", *J. Adhesion* **80**:4 (2004), 313–331.

[Rice and Levy 1972] J. R. Rice and N. Levy, "The part-through surface crack in an elastic plate", *J. Appl. Mech.* (*ASME*) **39** (1972), 185–194.

[Sensmeier and Wright 1989] M. D. Sensmeier and P. K. Wright, "The effect of fiber bridging on fatigue crack growth in titanium matrix composites", pp. 441 in *Fundamental relationships between microstructure and mechanical properties of metal-matrix composites*, edited by P. K. Liaw and M. M. Gungor, The Minerals, Metals and Materials Society, Indianapolis, 1989.

[Shetty and Spearing 1997] S. P. Shetty and S. M. Spearing, "Fracture resistance of a fiber-reinforced film adhesive", *Scr. Mater.* **37**:6 (1997), 787–792.

[Sorensen 2002] B. F. Sorensen, "Cohesive law and notch sensitivity of adhesive joints", *Acta Mater.* **50**:5 (2002), 1053–1061.

[Suo et al. 1993] Z. Suo, S. Ho, and X. Gong, "Notch ductile-to-brittle transition due to localized inelastic band", *J. Eng. Mater. Technol.* (*ASME*) **115**:3 (1993), 319–326.

[Tada et al. 1973] H. Tada, P. C. Paris, and G. R. Irwin, *The stress analysis of cracks handbook*, Del Research Corporation, Hellertown, PA, 1973.

[Tharp 1987] T. M. Tharp, "A finite element method for edge-cracked beam columns", *Int. J. Numer. Methods Eng.* **24**:10 (1987), 1941–1950.

[Wei and Hutchinson 1998] Y. Wei and J. W. Hutchinson, "Interface strength, work of adhesion and plasticity in the peel test", *Int. J. Fract.* **93**:1–4 (1998), 315–333.

[Wilson 1970] W. K. Wilson, "Stress intensity factors for deep cracks in bending and compact tension specimens", *Eng. Fract. Mech.* **2**:2 (1970), 168–171.

[Xu et al. 1995] H. H. K. Xu, C. P. Ostertag, E. R. Fuller, Jr., L. M. Braun, and I. K. Lloyd, "Fracture resistance of SiC-fiber-reinforced Si_3N_4 composites at ambient and elevated temperatures", *J. Am. Ceram. Soc.* **78**:3 (1995), 698–704.

[Yang and Ravi-Chandar 1996] B. Yang and K. J. Ravi-Chandar, "On the role of the process zone in dynamic fracture", *J. Mech. Phys. Solids* **44**:12 (1996), 1955–1976.

[Yang et al. 1999] Q. D. Yang, M. D. Thouless, and S. M. Ward, "Numerical simulations of adhesively-bonded beams failing with extensive plastic deformation", *J. Mech. Phys. Solids* **47**:6 (1999), 1337–1353.

[Yang et al. 2004] Q. D. Yang, D. J. Shim, and S. M. Spearing, "A cohesive zone model for low cycle fatigue life prediction of solder joints", *Microelectron. Eng.* **75**:1 (2004), 85–95.

[Yokoyama and Chen 1998] T. Yokoyama and M.-C. Chen, "Vibration analysis of edge-cracked beams using a line-spring model", *Eng. Fract. Mech.* **59**:3 (1998), 403–409.

[Young 1994] L.-J. Young, *A boundary element analysis of fracture surface and interference for mixed mode loading problems with elastic or plastic crack tips*, Ph.D. thesis, The Ohio State University, 1994.

[Zok and Hom 1990] F. Zok and C. L. Hom, "Large scale bridging in brittle matrix composites", *Acta Metall. Mater.* **38**:10 (1990), 1895–1904.

Received 30 Oct 2007. Revised 10 Jun 2008. Accepted 15 Aug 2008.

PRASAD S. MOKASHI: mokashi.1@osu.edu
Department of Mechanical Engineering, Scott Laboratory, The Ohio State University, 201 W 19th Avenue,, Columbus, Ohio 43210, United States

DANIEL A. MENDELSOHN: mendelsohn.1@osu.edu
Department of Mechanical Engineering, Scott Laboratory, The Ohio State University, 201 W 19th Avenue, Columbus, Ohio 43210, United States